CHEMISTRY
A EUROPEAN JOURNAL

DOI: 10.1002/chem.201100067

# Furan-Oxidation-Triggered Inducible DNA Cross-Linking: Acyclic Versus Cyclic Furan-Containing Building Blocks—On the Benefit of Restoring the Cyclic Sugar Backbone

Kristof Stevens,[a] Diederica D. Claeys,[b] Saron Catak,[b] Sara Figaroli,[a] Michal Hocek,[c] Jan M. Tromp,[d] Stefan Schürch,[d] Veronique Van Speybroeck,[b] and Annemieke Madder*[a]

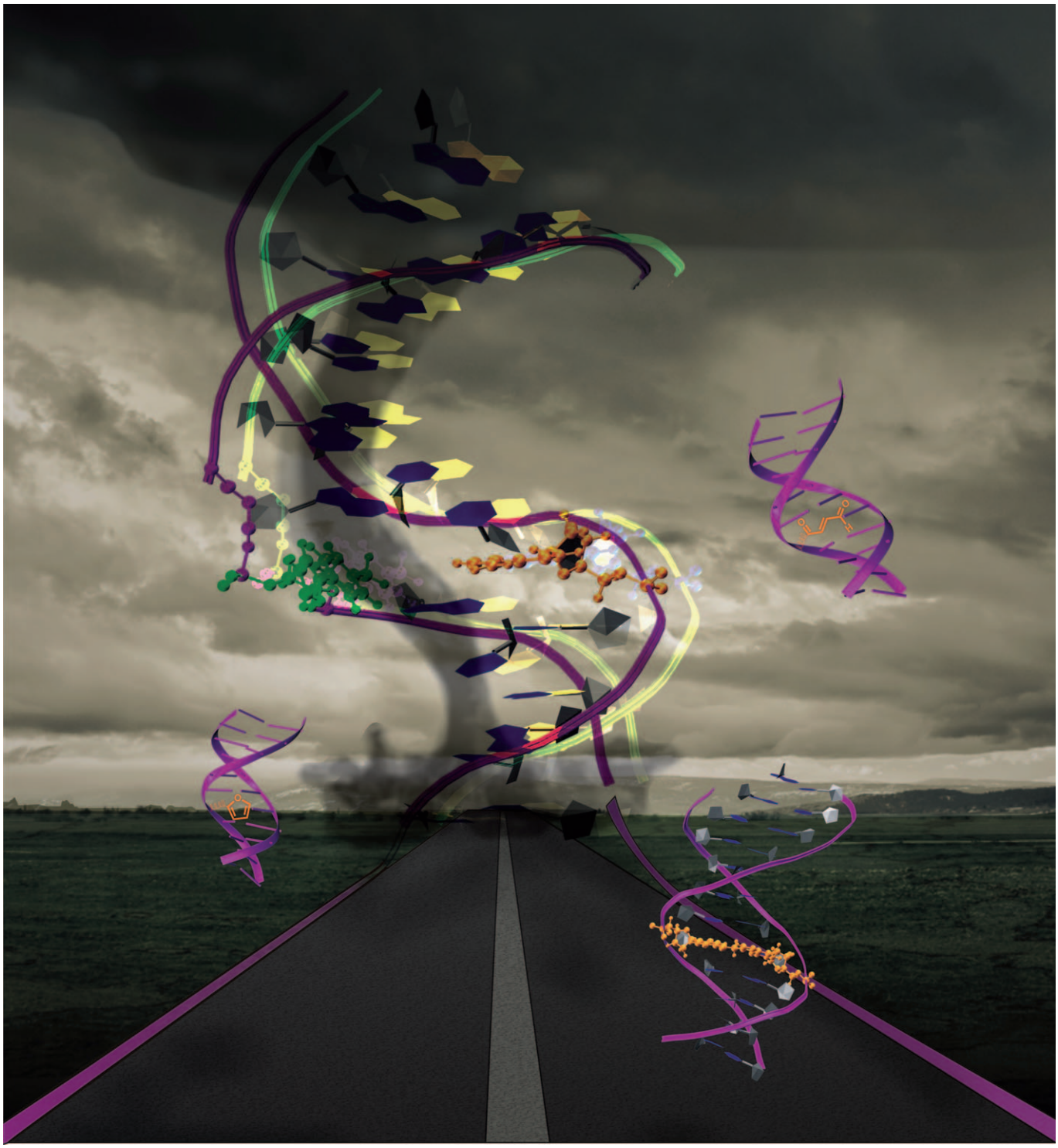

**Abstract:** Oligodeoxynucleotides incorporating a reactive functionality can cause irreversible cross-linking to the target sequence and have been widely studied for their potential in inhibition of gene expression or development of diagnostic probes for gene analysis. Reactive oligonucleotides further show potential in a supramolecular context for the construction of nanometer-sized DNA-based objects. Inspired by the cytochrome P450 catalyzed transformation of furan into a reactive enal species, we recently introduced a furan-oxidation-based methodology for cross-linking of nucleic acids. Previous experiments using a simple acyclic building block equipped with a furan moiety for incorporation into oligodeoxynucleotides have shown that cross-linking occurs in a very fast and efficient way and that substantial amounts of stable, site-selectively cross-linked species can be isolated. Given the destabilization of duplexes observed upon introduction of the initially designed furan-modified building block into DNA duplexes, we explore here the potential benefits of two new building blocks featuring an extended aromatic system and a restored cyclic backbone. Thorough experimental analysis of cross-linking reactions in a series of contexts, combined with theoretical calculations, permit structural characterization of the formed species and allow assessment of the origin of the enhanced cross-link selectivity. Our experiments clearly show that the modular nature of the furan-modified building blocks used in the current cross-linking strategy allow for fine tuning of both yield and selectivity of the interstrand cross-linking reaction.

**Keywords:** bioorganic chemistry · DNA · molecular modeling · nucleosides · oxidation

## Introduction

Furan is a chemical that has been found to be specifically hepatotoxic.[1–3] The mechanism of action involved in this toxicity rests on the cytochrome P450 mediated oxidation of the stable furan aromatic moiety into the reactive (*Z*)-2-butenedial, which is readily attacked by biological nucleophiles leading to a variety of deleterious adducts.[4–6] The study of its genotoxic effect and the underlying mechanism thereof continues to be an active area of interest and still needs to be completely understood.[7] Notwithstanding these toxic effects, furan has been identified as representing a caged reactive functionality and seems to be an ideal template for the mild and selective generation of a reactive intermediate on demand. This furan-ring oxidation principle and the idea of using an easily incorporated and stable aromatic furan moiety as a substitute for a reactive unit has been elegantly used in the total synthesis of macrosphelides A and B[8] and (+)-Aspicillin.[9] The principle was further applied in a combinatorial process for the generation of a large library of distinct molecular skeletons starting from a common 2-alkoxyfuran building block.[10]

Despite a few examples of its application both in total synthesis and in diversity-oriented synthesis, this furan oxidation strategy has never been exploited in a biological context before. Nevertheless, the furan moiety represents the ideal masked reactive functionality, offering the possibility for selective and on-demand triggering of its reactivity through oxidation, which can be achieved both in a chemical or an enzymatic way. We have therefore recently exploited this principle in the development of a novel furan-oxidation-based method for selective DNA interstrand cross-linking (ICL).[11,12]

Besides DNA interstrand cross-link repair, nucleotide excision repair, mismatch repair, base excision repair, and double-strand break repair are processes that are of paramount importance for the maintenance of our genome. The genomic material is constantly challenged and an average of 50000 DNA lesions per cell can be estimated to be produced on a daily basis. Detailed understanding of the natural defense mechanisms against DNA damage that is constantly being produced through exposure to, for example, sunlight, is necessary and hampered by the fact that among the above-cited repair processes, the mechanism of DNA cross-link repair still is considered to be a black box in our knowledge.[13] Indeed, the DNA damage induced by cross-linking the strands represents a formidable challenge to cell survival. As opposing strands are involved in the damage, these lesions are also very complex to process.[14] Human diseases such as Fanconi Anemia and Nijmegen breakage syndrome are characterized by a high sensitivity to DNA interstrand cross-links and predisposition to malignance and the basis of the basic defect in ICL repair remains unclear.[15] Next to the importance of a complete understand-

[a] Dr. K. Stevens, S. Figaroli, Prof. Dr. A. Madder
Laboratory for Organic and Biomimetic Chemistry
Department of Organic Chemistry, Ghent University
Krijgslaan 281, S4, 9000 Gent (Belgium)
Fax: (+32) 9-264-49-98
E-mail: Annemieke.Madder@UGent.be

[b] Dr. D. D. Claeys, Dr. S. Catak, Prof. Dr. V. V. Speybroeck
Center for Molecular Modeling, Ghent University
Technologiepark 903, 9052 Zwijnaarde (Belgium)

[c] Prof. Dr. M. Hocek
Institute of Organic Chemistry and Biochemistry
Academy of Sciences of the Czech Republic
Gilead Sciences & IOCB Research Center
Flemingovo nam. 2, 16610 Prague 6 (Czech Republic)

[d] Dr. J. M. Tromp, Prof. Dr. S. Schürch
Department of Chemistry and Biochemistry
University of Bern, Freiestrasse 3, 3012 Bern (Switzerland)

Supporting information for this article is available on the WWW under http://dx.doi.org/10.1002/chem.201100067.

  

ing of these mechanisms for the comprehension of natural repair processes, this knowledge is essential in the fight against resistance occurring in cancer treatments. Indeed, cross-link repair is known to be one of the major processes lying at the origin of resistance to anticancer chemotherapeutics and is still poorly understood.

The interest of ICL oligonucleotides lies in the possibility to generate substrates for a detailed study of cross-link repair in order to elucidate the mechanistic background for this phenomenon. Indeed, isolation of defined ICL adducts from natural sources in sufficient quantities for mechanistic studies remains a major problem[16] and treatment of DNA with external cross-linking reagents[17–22] typically yields complex mixtures of mono-adducts, and inter- and intrastrand cross-links with the desired ICLs are usually represented as minor fractions.[23] A variety of applications in the chemical biology area further justify the ongoing and intense research for efficient and highly sequence-specific cross-linked oligonucleotides. Next to increased antisense activity through irreversible binding to the target for specific knock down of particular mRNAs or miRNAs,[24] the interest of synthesis methods for the preparation of selectively cross-linked, small, double-stranded DNA sequences can further be found in the sequence-specific regulation of transcription factors by so-called decoy ODNs. ICLs have been shown to enhance decoy stability[25,26] and have the possibility to constrain the decoys into a more active conformation towards the target transcription factor.[27] Finally cross-linking of DNA can serve various purposes in structural biology and nanotechnology. Cross-linked DNA with an altered conformational behavior offers opportunities for understanding structure-specific DNA recognition in biological systems and in the development of nucleic acid based therapeutics.[28] A wealth of exotic and unfavorable DNA conformations has been restrained by cross-linking strategic parts. In addition to R-shaped DNA, n-, h-, and H-type DNA have been constructed in this way. Furthermore cross-linking hairpin termini can be used to continuously constrain the structure in the hairpin conformation.[29–31]

Bearing the problems associated with alkylating or reactive oligonucleotides and their instability in physiological media in mind, our recently developed cross-linking methodology is based on the use of a furan moiety as a stable precursor for reactive aldehyde functionality.[11] Relying on the inducible reactivity principle,[32] the furan moiety is oxidized selectively, after duplex formation, generating the cross-linking moiety in an environment in which the target nucleophiles are forced into proximity so as to minimize side reactions with non-target nucleophiles. Others have recently picked up this methodology and based on our furan-oxidation strategy have shown that such type of furan-containing probes can be used for the diagnosis of adenine-related DNA mutations.[33]

It has been recently illustrated that the exact chemical structure of an ICL can play a significant role in the repair processing of the cross-link.[34] Understanding how structurally different ICLs are repaired may provide a deeper understanding of the cytotoxic and mutagenic potential of specific ICLs. We therefore found it of importance to expand our previous studies towards furan-containing building blocks with a different chemical structure. Previous experiments were carried out using a building block connecting the furan moiety through an amido or ureido linker to the 2′-position of the sugar backbone.[11] In further studies we focussed our attention on an acyclic building block with the furan serving as base substitute.[12] Though significant influence on the modified duplex stability was observed, cross-link yields remained high. In view of this rather strong destabilization observed when incorporating the acyclic cross-linking building block into a DNA sequence, we now report on two new building blocks featuring an extended aromatic system for enhanced stacking interactions and considered both an acyclic and a cyclic sugar backbone. We here describe in detail a comparative study in which the benefits of an extended aromatic system were evaluated against the inclusion of a building block with restored cyclic sugar moiety. To fully understand the relation between the structure of the furan building blocks and the DNA ICL, in addition to the extensive experimental characterization of the formed species, various computational molecular modeling techniques have been applied.

## Results and Discussion

**Furan-oxidation exploited in a biological context—selective DNA interstrand cross-linking**: Recently, we have described the application of the furan-oxidation principle in a chemical biology context rather than the above-mentioned total synthesis. Oxidation of oligonucleotides incorporating an acyclic, furan-modified, building block results in the formation of an enal species that shows high reactivity towards cross-linking with the opposing base in the complementary strand (see Scheme 1 for illustration of the furan-oxidation-triggered cross-linking principle).[12]

Proximate nucleophilic functionality on the complementary DNA effectively quenches the reactive intermediate oxo–enal–oligonucleotide conjugate that is formed. Cross-linked duplexes can be isolated in high yields (up to 70% of isolated and purified cross-linked duplex) and were shown to be stable over extended periods of time.

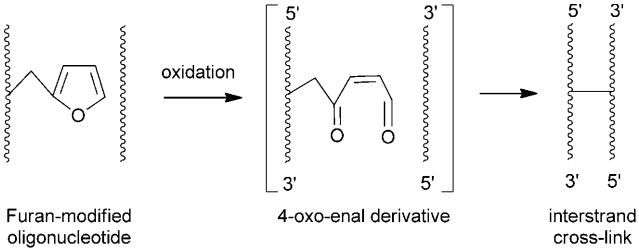


Scheme 1. Furan-oxidation triggered cross-linking of complementary oligodeoxyribonucleotides.

  

**Design considerations for improved building blocks**: For the incorporation of a furan unit into DNA duplex sequences, building block **1** (shown here) has been used in previous

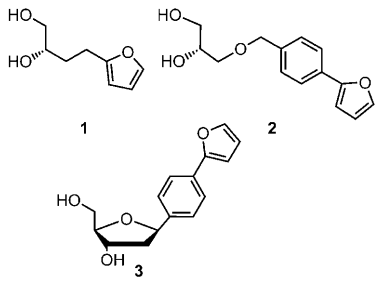

studies.[12] Interstrand cross-links are formed upon *N*-bromosuccinimide (NBS) oxidation of the incorporated furan moiety and it was observed that only the base which is complementary to the introduced modified nucleoside is involved in the covalent-bond formation. Strong selectivity for cross-linking to either a complementary adenine base or a complementary cytosine base has been demonstrated. The formed covalent interstrand link is stable and cross-linked duplexes can be stored for prolonged periods of time without degradation. However, duplexes incorporating modified building block **1** were between 17 and 28 °C less stable than the corresponding unmodified sequences. For antisense applications, this observed destabilization represents an important disadvantage. Moreover, in studies of the enzymatic mechanisms involved in cross-link repair, stability and structure of the duplex can play an important role for recognition of the synthetic substrate by the studied enzymes.

In an attempt to reduce destabilization of the duplex upon introduction of the furan modified residue, building blocks **2** and **3** were synthesized. We expect building block **2** to show enhanced stacking interactions and therefore influence duplex stability less, while reconstitution of the cyclic sugar moiety in **3** is expected to induce additional restriction of backbone flexibility and consequently cause less duplex destabilization.

**Synthesis of new furan modified building blocks**: Synthesis of building block **2** is outlined in Scheme 2. The first step involves $S_N2$ substitution of the 4-bromobenzyl bromide with commercially available (2,2-dimethyl-1,3-dioxolan-4-yl)methanol ((*S*)-solketal). Negishi cross-coupling of the aromatic bromide with furylzinc chloride completes the skeleton (**2**). Subsequent protection of the primary alcohol with dimethoxytrityl chloride should be carried out with care, as only a small difference in reactivity between the primary and secondary alcohol was observed. This results in formation of doubly dimethoxytritylated product, even when not all starting material is consumed. The highest selectivity could be obtained with a slight excess of the diol at low temperature. For the synthesis of phosphoramidite **7**, it was shown that in the case of similar glycerol nucleic acid modi-

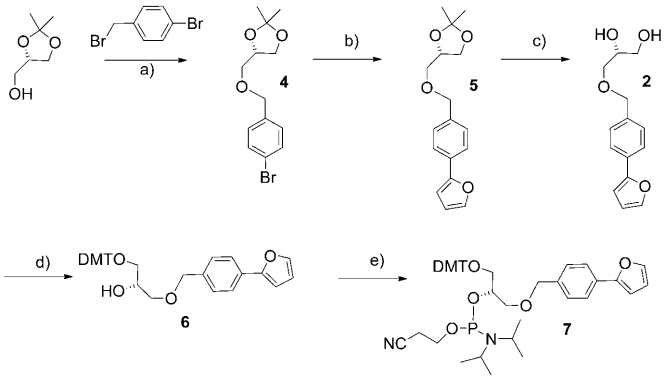

Scheme 2. Synthesis of phosphoramidite **7** required for incorporation of building block **2**. Reagents and conditions: a) KOH, toluene, Dean–Stark, 93% ; b) i) furan (10 equiv), *n*BuLi (9.5 equiv), $ZnCl_2$ (9.5 equiv), −78 to 0 °C; ii) $[Pd(PPh_3)_4]$ (0.03 equiv), 50 °C, 70%; c) HCl (4 M), THF, 0 °C, 97%; d) DMTCl (0.9 equiv), pyridine, 0 °C to RT, 73%; e) $(iPr_2N)_2(NCCH_2CH_2O)PCl$, diisopropylammonium tetrazolide (1.5 equiv), $CH_2Cl_2$, 0 °C to RT, 79%

fications, use of the standard β-cyanoethyl chlorophosphoramidite does not result in formation of the phosphoramidite. The less reactive β-cyanoethyl *N,N,N′,N′*-tetraisopropylphosphoramidite in the presence of diisopropylammonium tetrazolide as an activating species is used because of the mildness and chemoselectivity of this phosphitylation reaction. Building block **7** was thus obtained ready for incorporation into the desired oligonucleotide sequences.

The synthetic route for building block **3** was based on the modular approach[35–40] consisting in synthesis of halogenated aryl-C-nucleoside intermediate and its follow-up cross-coupling (Scheme 3). Protected bromophenyl-C-nucleoside **9** was prepared by a previously reported procedure[41,42] from halogenose **8** and 4-bromophenylmagnesium bromide. The Stille cross-coupling of **9** with 2-$Bu_3Sn$-furan gave the protected biaryl nucleoside **10** in excellent 88% yield. Standard deprotection under the Zemplen conditions gave the

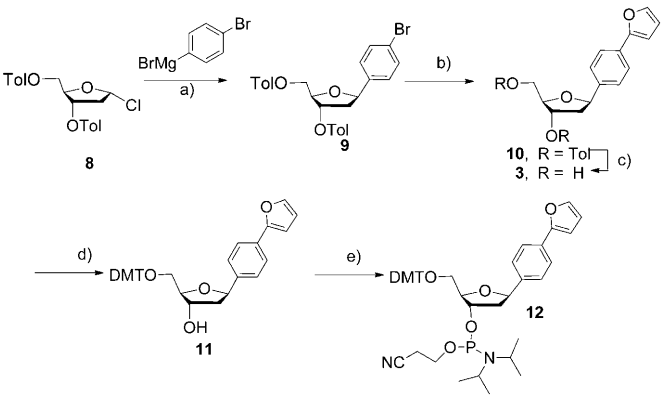

Scheme 3. Synthesis of phosphoramidite **12** required for incorporation of building block **3**. Reagents and conditions: a) Ref. [35]; b) 2-$Bu_3Sn$-furan, $[PdCl_2(dppf)]$, DMF, 100 °C, 16 h, 88%; c) NaOMe, MeOH, RT, 85%; d) DMTCl (1.5 equiv), pyridine, 0 °C to RT, 66%; e) $(iPr_2N)(NCCH_2CH_2O)PCl$, *N,N*-diisopropylethylamine, $CH_2Cl_2$, RT, 59%

  

desired furylphenyl C-nucleoside **3**. Transformation into the protected phosphoramidite **12** was in this case achieved with the standard β-cyanoethyl chlorophosphoramidite and furnished the correct building block for automated DNA synthesis.

**Oligonucleotide synthesis and purification**: To allow detailed evaluation of cross-link selectivity and influence of the sequence context, building blocks **2** and **3** were incorporated into a series of four different sequences varying the neighboring bases (see Table 1, below). Incorporation of **2** into oligonucleotides was carried out by automated DNA synthesis in accordance with methods previously described.[12] 4,5-Dicyanoimidazole in acetonitrile was added as activator.[43] Coupling of the modified nucleoside was performed manually with a prolonged coupling time of 10 min. The coupling yields under these conditions were estimated to be more than 99%. DMT-groups were left on the terminal 5′-position in order to allow purification by Sep-pak filtration. As for sequences incorporating modified building block **3**, again manual couplings and 4,5-dicyanoimidazole activation were applied. However, coupling yields using **12** were much lower as compared to the acyclic building block. In this case, the estimated coupling yield resided around 80% based on trityl group release. Further extension of the chain was not hampered and synthesis could be continued with standard good coupling yields. Analysis data for all synthesized oligonucleotides can be found in Supporting Information.

**Thermal analysis of modified duplexes**: To allow detailed evaluation of cross-link selectivity each of the oligonucleotides was paired with four different complements varying the opposing base. Table 1 summarizes melting point results for duplexes incorporating the modified building blocks.

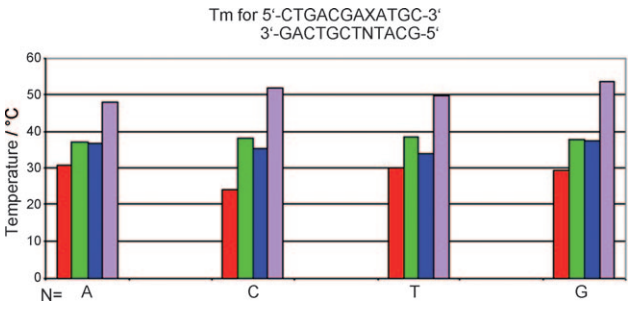


Figure 1. Comparative graph of melting temperatures for duplexes incorporating building blocks **1**, **2**, and **3**. (Example shown for 5′-CTGACGAXATGC-3′:3′-GACTGCTNTACG-5′, with X = **1**, **2**, **3** or the complement to N (from left to right in each block) and N = A, C, T or G).

Table 1. Melting temperatures [in °C] of duplexes modified with nucleoside building blocks **2** and **3** ($\Delta T_m$ values between brackets refer to fully complementary reference duplexes without **2** or **3**). Recorded at 260 nm, 2 μM duplex concentration, 10 mM phosphate buffer pH 7 and 100 mM NaCl.

| Modified strand\ Complementary base | A $T_m$ ($\Delta T_m$) | C $T_m$ ($\Delta T_m$) | T $T_m$ ($\Delta T_m$) | G $T_m$ ($\Delta T_m$) |
|---|---|---|---|---|
| **ON1**: 5′-CTG ACG G**2**G TGC-3′ | 45.2 (−11.5) | 48.9 (−10.4) | 45.1 (−8.0) | 45.6 (−16.8) |
| **ON2**: 5′-CTG ACG C**2**C TGC-3′ | 41.9 (−11.8) | 41.3 (−20.3) | 47.6 (−8.7) | 46.2 (−12.5) |
| **ON3**: 5′-CTG ACG A**2**A TGC-3′ | 36.9 (−11.2) | 38.3 (−13.7) | 38.4 (−11.3) | 37.9 (−15.5) |
| **ON4**: 5′-CTG ACG T**2**T TGC-3′ | 35.0 (−14.7) | 35.6 (−17.9) | 34.5 (−12.7) | 36.4 (−15.3) |
| **ON5**: 5′-CTG ACG G**3**G TGC-3′ | 44.4 (−12.3) | 47.1 (−12.1) | 40.1 (−13.0) | 45.3 (−17.1) |
| **ON6**: 5′-CTG ACG C**3**C TGC-3′ | 40.4 (−13.3) | 39.9 (−21.7) | 41.4 (−14.9) | 43.4 (−15.3) |
| **ON7**: 5′-CTG ACG A**3**A TGC-3′ | 36.7 (−11.4) | 35.4 (−16.6) | 34.0 (−15.7) | 37.8 (−15.6) |
| **ON8**: 5′-CTG ACG T**3**T TGC-3′ | 34.7 (−15.0) | 32.6 (−20.9) | 33.8 (−13.4) | 37.2 (−14.5) |

Graphical representation of this melting point analysis illustrates more clearly that with respect to the previous generation of duplexes incorporating building block **1**, stabilization can be observed when incorporating an extra phenyl unit as in building block **2** (Figure 1).[44]

As illustrated, the extra stabilization expected for a restored entirely cyclic backbone was absent. Duplexes incorporating **3** were, in most cases, even somewhat lower in stability. Whereas building block **2** benefits from enhanced stacking interactions resulting from the increased aromatic surface (when compared to **1**), restriction of conformational flexibility and restoration of the backbone in building block **3** does not result in an increased duplex stability.

To obtain a more profound understanding of these relations between the structure of the various building blocks and the overall stability, molecular dynamic simulations with implicit solvent were performed in AMBER 9.[45,46] The computational details are given in the Supporting Information. Modeling of the **ON1** and **ON5** series shows a very similar behavior for both biaryl modifications, irrespective of the complementary base. Incorporation of the phenyl–furan nucleoside into the duplex opposite to a purine or pyrimidine nucleobase causes local disruption of the stacking. Most of the time, the phenyl–furan moiety is forced into the major groove, but has an inner helical position that allows the modification to stack with its 5′ base. The modified duplexes rarely form interstrand stacked zip-like arrangements. The modification is too large to be accommodated in one plane with its complement and, apparently, to form an intercalating structure, the aromatic part of the modification is too small to provide a stable interstrand stacked pair.

This is illustrated in Figure 2 which shows two representative snapshots from the molecular dynamics simulations performed on **D2a** and **D3a** (see Table 2) with a complementary adenine base. Similar results have been reported in literature for a biphenyl modification flanked at both sides by a C·G base pair[47] and have been deduced from an experimental fluorescence study for the biphenyl modification flanked by an A·T and a C·G base pair.[48]

  

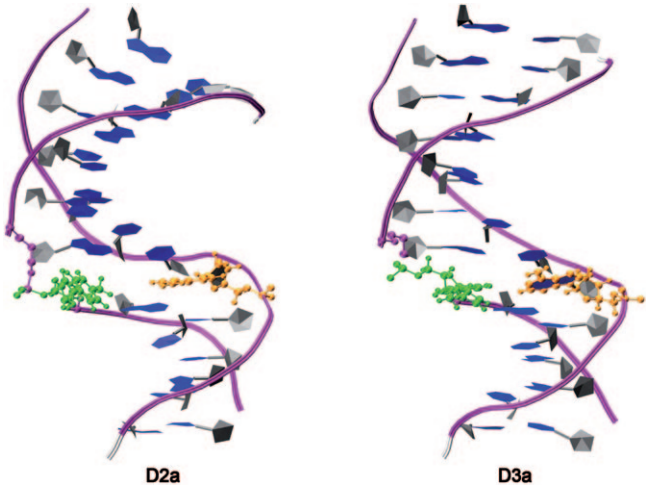


Figure 2. Representative samples of the **D2a** (core $G_7\mathbf{2}G_9{:}C_{18}A_{17}C_{16}$) and **D3a** (core $G_7\mathbf{3}G_9{:}C_{18}A_{17}C_{16}$) simulations show the modification (in green) that rarely forms an interstrand stacked pair, but resides in the major groove of the locally distorted double helix. The complementary adenine base (in orange) shows π-stacking with its 5′ base.

Simulations of **D2i** and **D3i** show that duplex **D3i** with a restored cyclic backbone has more often a zip-like conformation, while modification **2** rarely forms an intercalated structure. An example of this intercalating conformation with the cyclic modification **3** is given in Figure 3.

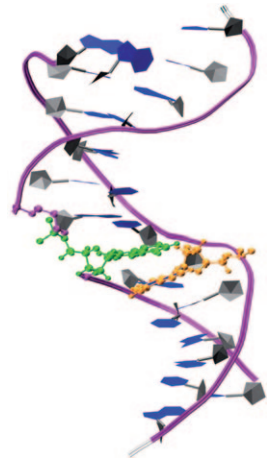

Figure 3. Example of an intercalating zip-like structure of modification **3** (in green) between its complementary base (in orange) and the Crick 3′ base taken from the simulation of **D3i** (core $A_7\mathbf{3}A_9{:}T_{18}A_{17}T_{16}$).

Also the duplexes **D3f** and **D3e** have more often an intercalated zip-like conformation, which correlates with the number of purine bases at positions 16, 17, and 18, as these have a more extended aromatic system. Again, this is not observed for modification **2**. It is clear that an optimal intercalating alignment of the extended aromatic phenyl–furan modification in building blocks **2** and **3** is hampered. Only a π-stacking interaction, mainly with the Watson 5′ base can be formed. If modification **3** is flanked by base pairs that form only two hydrogen bridges, zip-like intercalating structures can be formed at the expense of duplex stabilization by hydrogen bonds and probably also π-stacking (see Table S3 in Supporting Information for details). This explains the lack of enhancement of the duplex stability by restoration of the cyclic backbone in modification **3**.

**Interstrand cross-link formation and selectivity**: We next investigated the cross-link performance and selectivity within this new series of oligonucleotides incorporating the new furan-modified building blocks (see Table 2). Cross-link experiments were carried out as previously described[12] by mixing equimolar amounts of the furan-modified and complementary non-modified oligonucleotides in a 1:1 ratio, followed by controlled addition of NBS. In contrast to the recently developed methodology of Schärer,[23] but similar to cross-linking occurring at abasic sites,[49] no extra reductive amination step is necessary to ensure stable cross-link formation. The mere NBS treatment of the mixture of modified and complementary oligonucleotide in the current study results in the formation of cross-linked products that are stable and can be analyzed by using both HPLC and MALDI-TOF methods.

Cross-linking occurs instantaneously after NBS addition, and upon analysis of the reaction mixture two new species can be observed in the reverse-phase HPLC chromatogram. Figure 4 shows reverse-phase HPLC analysis data for the specific case of duplex **D2a** cross-linking, before (Fig-

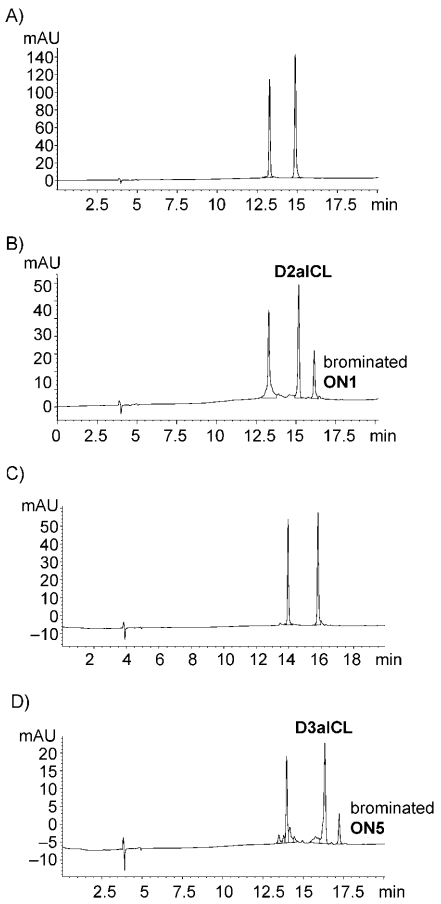


Figure 4. Reverse-phase HPLC chromatogram for cross-linking of duplex **D2a** (**ON1**+**ON9**, core $G_7\mathbf{2}G_9{:}C_{18}A_{17}C_{16}$) and **D3a** (**ON5**+**ON9**, core $G_7\mathbf{3}G_9{:}C_{18}A_{17}C_{16}$) before addition of NBS (chromatogram A and C respectively) and after addition of four equivalents of NBS (B and D respectively). All **ON** sequences are mixed in a 1:1 ratio. **D2aICL** and **D3aICL** designate the formed cross-linked species.

Table 2. Sequences of modified duplexes incorporating building blocks **2** and **3**. Modified nucleosides are designated by X, variable nucleosides are designated by N. Specific identity of the core sequences is specified for each duplex incorporating **2** (left column) and **3** (right column).

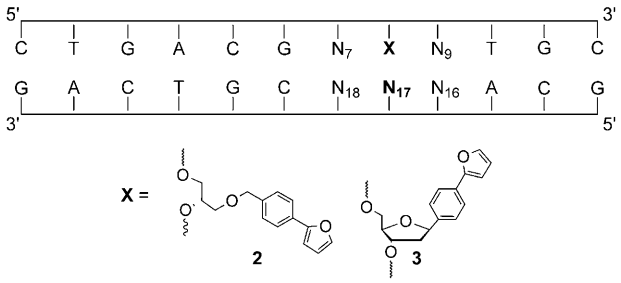


| Duplex | $N_7$ | **2** | $N_9$ | Duplex | $N_7$ | **2** | $N_9$ | Duplex | $N_7$ | **3** | $N_9$ | Duplex | $N_7$ | **3** | $N_9$ |
|---|---|---|---|---|---|---|---|---|---|---|---|---|---|---|---|
| | $N_{18}$ | $\mathbf{N_{17}}$ | $N_{16}$ | | $N_{18}$ | $\mathbf{N_{17}}$ | $N_{16}$ | | $N_{18}$ | $\mathbf{N_{17}}$ | $N_{16}$ | | $N_{18}$ | $\mathbf{N_{17}}$ | $N_{16}$ |
| **D2a** | | | | **D2i** | | | | **D3a** | | | | **D3i** | | | |
| ON1 | $G_7$ | **2** | $G_9$ | ON3 | $A_7$ | **2** | $A_9$ | ON5 | $G_7$ | **3** | $G_9$ | ON7 | $A_7$ | **3** | $A_9$ |
| ON9 | $C_{18}$ | $\mathbf{A_{17}}$ | $C_{16}$ | ON17 | $T_{18}$ | $\mathbf{A_{17}}$ | $T_{16}$ | ON9 | $C_{18}$ | $\mathbf{A_{17}}$ | $C_{16}$ | ON17 | $T_{18}$ | $\mathbf{A_{17}}$ | $T_{16}$ |
| **D2b** | | | | **D2j** | | | | **D3b** | | | | **D3j** | | | |
| ON1 | $G_7$ | **2** | $G_9$ | ON3 | $A_7$ | **2** | $A_9$ | ON5 | $G_7$ | **3** | $G_9$ | ON7 | $A_7$ | **3** | $A_9$ |
| ON10 | $C_{18}$ | $\mathbf{C_{17}}$ | $C_{16}$ | ON18 | $T_{18}$ | $\mathbf{C_{17}}$ | $T_{16}$ | ON10 | $C_{18}$ | $\mathbf{C_{17}}$ | $C_{16}$ | ON18 | $T_{18}$ | $\mathbf{C_{17}}$ | $T_{16}$ |
| **D2c** | | | | **D2k** | | | | **D3c** | | | | **D3k** | | | |
| ON1 | $G_7$ | **2** | $G_9$ | ON3 | $A_7$ | **2** | $A_9$ | ON5 | $G_7$ | **3** | $G_9$ | ON7 | $A_7$ | **3** | $A_9$ |
| ON11 | $C_{18}$ | $\mathbf{T_{17}}$ | $C_{16}$ | ON19 | $T_{18}$ | $\mathbf{T_{17}}$ | $T_{16}$ | ON11 | $C_{18}$ | $\mathbf{T_{17}}$ | $C_{16}$ | ON19 | $T_{18}$ | $\mathbf{T_{17}}$ | $T_{16}$ |
| **D2d** | | | | **D2l** | | | | **D3d** | | | | **D3l** | | | |
| ON1 | $G_7$ | **2** | $G_9$ | ON3 | $A_7$ | **2** | $A_9$ | ON5 | $G_7$ | **3** | $G_9$ | ON7 | $A_7$ | **3** | $A_9$ |
| ON12 | $C_{18}$ | $\mathbf{G_{17}}$ | $C_{16}$ | ON20 | $T_{18}$ | $\mathbf{G_{17}}$ | $T_{16}$ | ON12 | $C_{18}$ | $\mathbf{G_{17}}$ | $C_{16}$ | ON20 | $T_{18}$ | $\mathbf{G_{17}}$ | $T_{16}$ |
| **D2e** | | | | **D2m** | | | | **D3e** | | | | **D3m** | | | |
| ON2 | $C_7$ | **2** | $C_9$ | ON4 | $T_7$ | **2** | $T_9$ | ON6 | $C_7$ | **3** | $C_9$ | ON8 | $T_7$ | **3** | $T_9$ |
| ON13 | $G_{18}$ | $\mathbf{A_{17}}$ | $G_{16}$ | ON21 | $A_{18}$ | $\mathbf{A_{17}}$ | $A_{16}$ | ON13 | $G_{18}$ | $\mathbf{A_{17}}$ | $G_{16}$ | ON21 | $A_{18}$ | $\mathbf{A_{17}}$ | $A_{16}$ |
| **D2f** | | | | **D2n** | | | | **D3f** | | | | **D3n** | | | |
| ON2 | $C_7$ | **2** | $C_9$ | ON4 | $T_7$ | **2** | $T_9$ | ON6 | $C_7$ | **3** | $C_9$ | ON8 | $T_7$ | **3** | $T_9$ |
| ON14 | $G_{18}$ | $\mathbf{C_{17}}$ | $G_{16}$ | ON22 | $A_{18}$ | $\mathbf{C_{17}}$ | $A_{16}$ | ON14 | $G_{18}$ | $\mathbf{C_{17}}$ | $G_{16}$ | ON22 | $A_{18}$ | $\mathbf{C_{17}}$ | $A_{16}$ |
| **D2g** | | | | **D2o** | | | | **D3g** | | | | **D3o** | | | |
| ON2 | $C_7$ | **2** | $C_9$ | ON4 | $T_7$ | **2** | $T_9$ | ON6 | $C_7$ | **3** | $C_9$ | ON8 | $T_7$ | **3** | $T_9$ |
| ON15 | $G_{18}$ | $\mathbf{T_{17}}$ | $G_{16}$ | ON23 | $A_{18}$ | $\mathbf{T_{17}}$ | $A_{16}$ | ON15 | $G_{18}$ | $\mathbf{T_{17}}$ | $G_{16}$ | ON23 | $A_{18}$ | $\mathbf{T_{17}}$ | $A_{16}$ |
| **D2h** | | | | **D2p** | | | | **D3h** | | | | **D3p** | | | |
| ON2 | $C_7$ | **2** | $C_9$ | ON4 | $T_7$ | **2** | $T_9$ | ON6 | $C_7$ | **3** | $C_9$ | ON8 | $T_7$ | **3** | $T_9$ |
| ON16 | $G_{18}$ | $\mathbf{G_{17}}$ | $G_{16}$ | ON24 | $A_{18}$ | $\mathbf{G_{17}}$ | $A_{16}$ | ON16 | $G_{18}$ | $\mathbf{G_{17}}$ | $G_{16}$ | ON24 | $A_{18}$ | $\mathbf{G_{17}}$ | $A_{16}$ |

ure 4A) and after (Figure 4B) complete oxidation of modified **ON1**. In addition to the characterization of remaining unmodified strand (eluting first in both cases), MALDI-TOF MS analysis confirmed the cross-linked nature of the compound eluting at 15.175 min (see Supporting Information for detailed MS analysis of all cross-link reaction mixtures). As described earlier, furan-based cross-linking within a duplex can give rise to two different cross-linked species that co-elute. In addition to a mass corresponding to the mere sum of $\mathbf{ON1}_{oxidized}+\mathbf{ON9}$, a second mass corresponding to a dehydration product of this cross-linked compound can be deduced. The last compound eluting at 16.133 min was shown to correspond to a brominated derivative of **ON1**. A similar behavior during cross-link reactions was observed in case of cyclic building block **3** modified duplexes. Besides the remaining unmodified starting strand, a cross-linked product was characterized and again a small percentage of the brominated modified strand **ON5** was detected.

To get an overview of cross-link selectivity, the systematic variation of flanking and opposing bases resulted in cross-linking experiments with a series of 16 duplexes each for building blocks **2** and **3**. Gel electrophoresis analysis gives a quick and clear idea of the overall selectivity of the cross-link reaction in terms of the influence of the identity of the opposing and neigboring bases on the cross-link outcome (Figure 5). In the case of building block **2**, cross-link formation occurs to complementary C or A bases, while in case of complementary G or T, no major cross-linked species are formed. This behavior is analogous to the cross-link performance of the first-generation building block **1**.

However, for building block **3**, a much more pronounced C selectivity can be observed. Clear cross-linking to both A and C is only observed (lane 2 and 4) when **3** is flanked by two G residues (duplexes **D3a**–**D3d)**; in the other flanking contexts, only in case of a C base opposite **3** can a clear cross-linked species be visualized (see lanes 9, 14, and 19 for a clear spot related to ICL product; lanes 7, 12 and 17 only show a minor trace of cross-linked product).

This more pronounced C preference over A was also investigated by molecular dynamic simulations of **D2m**, **D2n**, **D3m**, and **D3n**. Although a furan moiety was used instead of the reacting 4-oxobutenal, these simulations give a first indication to explain the selectivity, as stacking occurs very often through the phenyl ring of the modification. With T·A neighboring base pairs, the hydrogen bridges are more easily broken to accommodate the modification in a zip-like structure. During the simulation of modification **3** and a complementary A base, the phenyl–furan moiety had a zip-like intercalating conformation (Figure 6A) or showed π-stacking with its 5′ base (Figure 6B). This more defined position of the furan ring could hamper correct positioning of

  

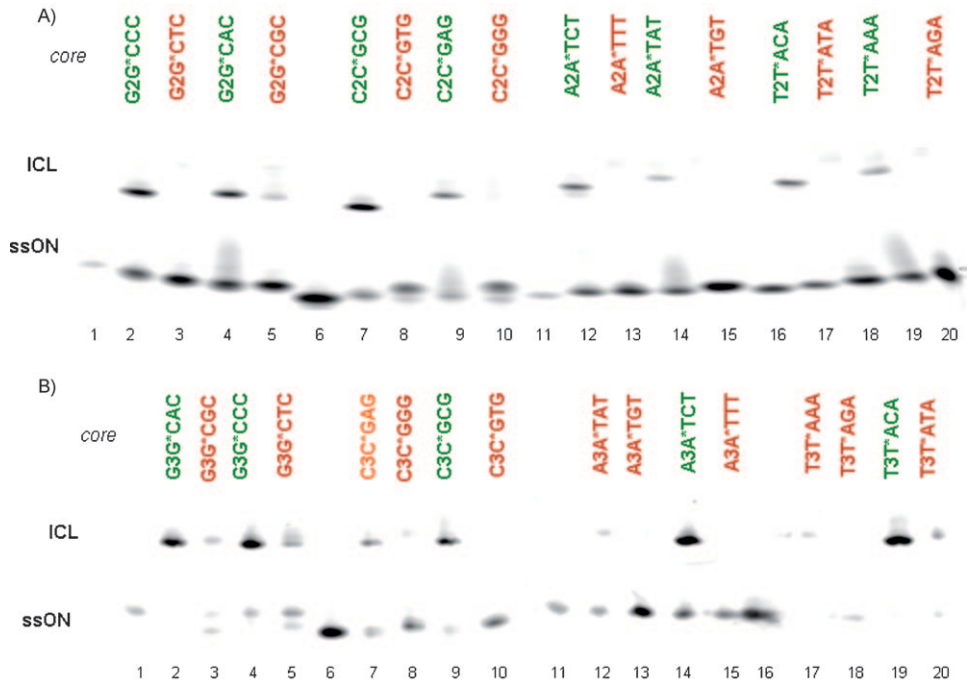


Figure 5. Denaturing PAGE results of the cross-link reaction with **2** and **3**. Furan-containing **ON1–8** were annealed to the different complements in a 1:1 ratio to obtain duplexes **D2a–D2d** (A, lanes 2–5), **D2e–D2h** (A, lanes 7–10), **D2i–D2l** (A, lanes 12–15), **D2m–D2p** (A, lanes 17–20), and **D3a–D3d** (B, lanes 2–5), **D3e–D3h** (B, lanes 7–10), **D3i–D3l** (B, lanes 12–15) and **D3m–D3p** (B, lanes 17–20), after which NBS was added in portions. ICL formation was analyzed by 20% denaturing PAGE. Lanes 1, 6, 11, and 16 refer to single-strand references.

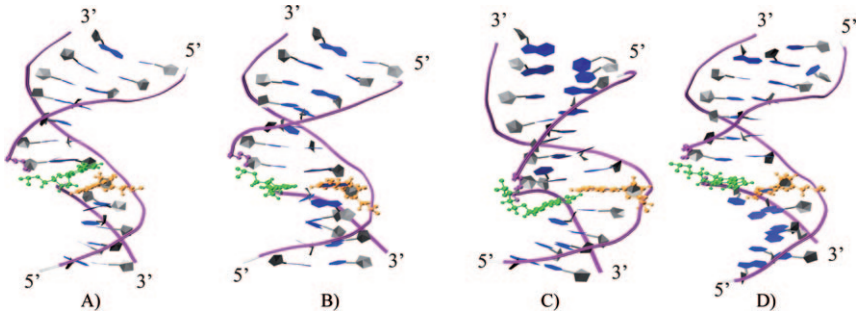


Figure 6. Snapshots of the simulation of **D3m** and **D2m** showing the more rigid position of modification **3** and the more flexible modification **2**. Complementary bases are represented in orange, furan-modified building blocks in yellow: A) duplex **D3m** (core $T_7\mathbf{3}T_9$:$A_{18}A_{17}A_{16}$) showing intercalated **3** and distant from $NH_2$ of $A_{17}$; B) duplex **D3m** (core $T_7\mathbf{3}T_9$:$A_{18}A_{17}A_{16}$) showing **3** stacked with its 5′ neighbor and distant from $NH_2$ of $A_{17}$; C) duplex **D2m** (core $T_7\mathbf{2}T_9$:$A_{18}A_{17}A_{16}$) showing **2** residing in the major groove in good position for attack by $NH_2$ of $A_{17}$; D) duplex **D3n** (core $T_7\mathbf{3}T_9$:$A_{18}C_{17}A_{16}$) showing **3** stacked with its 5′ neighbor and in good position for attack by $NH_2$ of $C_{17}$.

the complement for attack to the generated oxo–enal functionality and inhibit cross-linking to A, whereas the more flexible modified building block **2** allows cross-link formation (Figure 6C). The smaller pyrimidine C complement shows less π-stacking interaction with the phenyl–furan moiety. For about 50% of the simulation time, modification **3** stacks with its 5′ base or forms zip-like structures; during the other half it resides in the major groove. This less-defined position allows cross-link formation. Cross-linking can occur if the phenyl–furan moiety adopts a non-stacking inner helical position or when it stacks with its 5′ base, as illustrated in Figure 6D. Another explanation could be that the $NH_2$ group on the pyrimidine base has a better cross-linking position than on the purine base.

Reverse-phase HPLC analysis of all cross-linking reactions revealed the same trends in selectivity for complementary bases. Both cross-linking to A and C is consistently observed for duplexes incorporating **2**. Similar to observations at the gel electrophoresis stage, for duplexes incorporating **3**, a higher C selectivity is confirmed and only in case of duplex **D3a** ($G_7\mathbf{3}G_9$:$C_{18}\mathbf{A}_{17}C_{16}$ sequence context), a small amount of duplex cross-linked to A can be observed and characterized. All cross-linked species were isolated and analyzed by UV–denaturation experiments to determine their stability. It was shown that all cross-linked duplexes are stable when stored over longer time periods and display a melting point of around 70–80°C (see Supporting Information for detailed data and corresponding curves). Isolated yields of purified cross-linked duplexes range from 10–30% (see Supporting Information for details). Considering that only one equivalent of the opposing strands is used, the isolated yields of specifically cross-linked duplex are still impressive when comparing to previously published procedures. Moreover increased equivalents of either modified or target strand should easily allow the isolation of larger amounts of specifically cross-linked species for ICL repair studies. It should be noted that these yields are lower than our previously reported yields for cross-link formation using **1**. This can clearly be attributed to the formation of the brominated side product. As no brominated species were observed by using cross-link moiety **1** and all brominated species were observed as single strands, apparently the bromination of the modified oligonu-

  

cleotides excludes further cross-link formation. We therefore embarked on the detailed characterization of the brominated species.

**Characterization of brominated side products**: For the purpose of facilitating identification of the brominated species, cross-link experiments were performed on a shorter model **D2q** (shown in Figure 7, left) and the brominated single-stranded species (Figure 7, right) was isolated and analyzed.

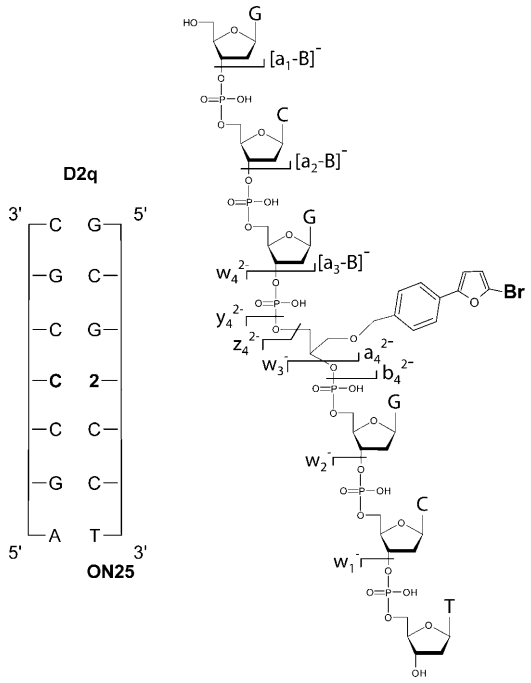


Figure 7. Indicative fragment ions for determination of the bromination site within the 7-mer single strand **ON25Br** (2195.3 Da). The $[M-4H]^{4-}$ ion ($m/z$ 547.8) was selected as the precursor for collision-induced dissociation on a hybrid quadrupole time-of-flight mass spectrometer (Applied Biosystems QStar Pulsar). Fragment ions, which do not incorporate the modified building block ($w_1^-$, $w_2^-$, $w_3^-$, $[a_1\text{-B}]^-$, $[a_2\text{-B}]^-$, and $[a_3\text{-B}]^{2-}$) give no evidence for the presence of any bromine atom. Fragment ions incorporating the modified residue ($a_4^{2-}$, $b_4^{2-}$, $w_4^{2-}$, $y_4^{2-}$, and $z_4^{2-}$) all show the bromine-typical isotopic pattern and mass shift.

Localization of the bromination site was performed by nanoelectrospray tandem mass spectrometry on a hybrid quadrupole-time-of-flight instrument. Multiply deprotonated single strands were selected as precursor ions for subsequent collision-induced dissociation. The corresponding product ion spectra provide complete sequence information of the single strands due to the presence of abundant [a-B]- and w-ion series, which are generated by cleavage of the oligonucleotide backbone at the 3′-C–O bonds. Such dissociation behavior is in agreement with the generally accepted gas-phase dissociation mechanism of oligodeoxynucleotides.[50]

Bromine-containing fragment ions are easily recognized by their characteristic isotopic pattern and the mass shift caused by the halogen substituent. For all brominated single strands analyzed, no bromine-containing [a-B] ions originating from the 5′-side of the modified residue are observed, and identical observations are made for the w ions originating from the 3′-side of the modification. Consequently, the bromine atom must reside on the modified residue exclusively. Incorporation of the modified building block into the single strand promotes backbone cleavage at alternative positions, resulting in additional fragment ions that provide more information about the bromination site. In the product ion spectrum of the brominated 7-mer single chain, the presence of bromine-containing $a_4^{2-}$, $b_4^{2-}$, $y_4^{2-}$, and $z_4^{2-}$ ions due to backbone cleavage adjacent to the modified residue is additional unambiguous evidence for the bromination site (Figure 7).

The most susceptible site for furan bromination in the modified residue is C2 (Scheme 4). Initial attack of the electrophilic bromine generates an oxonium species, which can

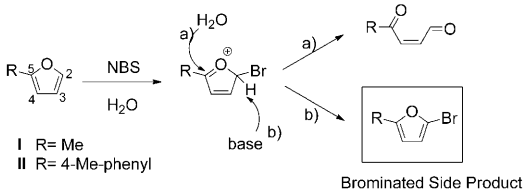


Scheme 4. Proposed mechanism for bromination studied on minimized structures **I** and **II** with methyl and 4-methylphenyl substituted furan.

be attacked by an $H_2O$ molecule and further oxidized by expelling the bromine (pathway a).[51] If water attack on C5 is disfavored, a side reaction that was previously proposed by Kishihara et al.[52] may occur; that is, abstraction of the C2 proton by a neighboring base. This will generate the brominated furan moiety, which remains insensitive to further oxidative ring-opening, thus interfering with the cross-linking process (pathway b). As brominated species were observed in the case of building blocks **2** and **3**, but not for **1**, theoretical calculations were performed as to elucidate the role of the phenyl moiety in the reaction with NBS. As this part of the simulations involves the localization of reactive pathways, density functional theory based calculations were performed as explained in detail in the Supporting Information. Bromination could be attributed to the increased stability of the phenyl conjugated furan oxonium species, for which water attack on C5 is disfavored, since it will disrupt extended conjugation. An increased barrier for furan oxidation would then allow the side reaction a competitive chance and result in brominated side products.

To rationalize the formation of the brominated side product, the difference in ease of furan oxidation has been investigated by density functional theory for structures **I** and **II**, in which methyl and 4-methylphenyl side chains, respectively, were used to model the rate-determining step.[51] These theoretical calculations have further validated the difference in ease of water attack on the oxonium species in the non-conjugated (**I**) versus phenyl-conjugated systems (**II**), showing significantly higher barriers for the latter. Details of the

  

computational methodology can be found in Supporting Information. More specifically, energy profiles and transition-state geometries for water attack on the furan oxonium are depicted in Figure 8. TS-Me and TS-Tol are both "product-like" and have similar critical distances; however, they differ remarkably (approximately 40 kJ mol$^{-1}$) with respect to their activation barriers. This is due to the extra stability of the phenyl-conjugated furan; hence, the barrier to attack is higher since conjugation is disturbed in the transition state (TS-Tol). As a consequence, the side reaction (Scheme 4, pathway b), which restores aromaticity through proton abstraction at C2 becomes competitive and brominated side products may form. An alternative mechanism leading to brominated species via a bromohydrin intermediate is also possible (see Supporting Information for more details).

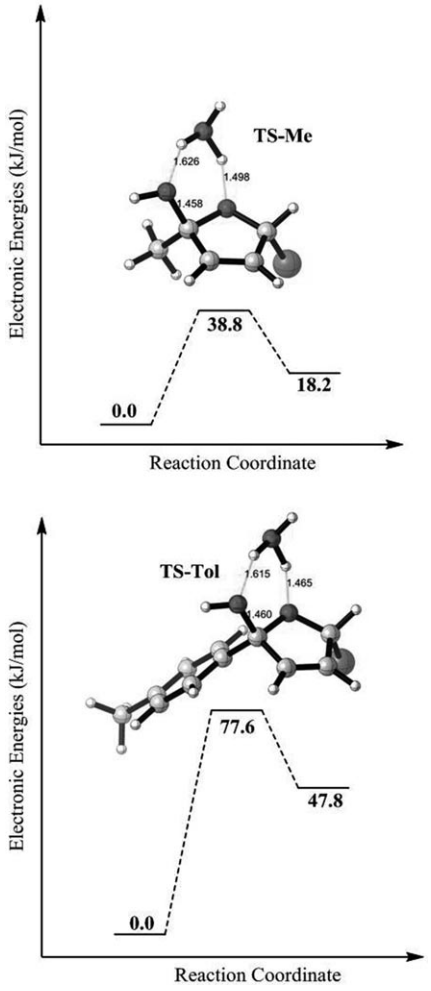


Figure 8. Reaction profile (MP2/6-31+G(d,p)//B3LYP/6-31+G(d,p)) and transition states for the hydrolysis of the intermediates arising from the bromination of **I** (above) and **II** (below) with two water molecules.

**Localization of the cross-linked site—enzymatic digestion studies**: With the characterization of the major side product accomplished, we now turned our attention to the actual species of interest, the cross-linked duplexes. Enzymatic degradation studies using exonuclease III (EXO III) on isolated cross-linked species were employed to allow the localization of the exact position of the cross-linking bond. The observed cleavage pattern indicating inhibition of the EXO III by the presence of the cross-link is consistent with earlier results showing that EXO III activity is inhibited by ethenoadenine up to and beyond the position of its occurrence in ds DNA.[53]

A typical reverse-phase HPLC outcome of cross-linked duplex digestion by EXO III is shown in Figure 9 for the specific case of duplex **D2a**. As illustrated by this analysis, digestion occurs up to two bases before the position of the modified building block in the modified strand. Digestion is further hampered in the non-modified complementary strand, as in addition to fragments containing most of the modified strand covalently connected to an A residue (Figure 9a), cross-linked fragments containing a 5′-tail can also be isolated (Figure 9b).

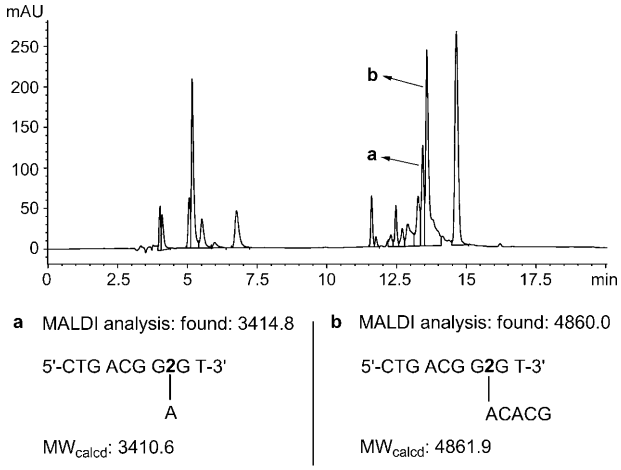


Figure 9. Reverse-phase HPLC chromatogram after EXO III digestion of duplex **D2a** d(CTGACGG**2**GTGC:GACTGCCACACG). Enzymatic degradation was performed using 200 units of EXOIII for purified cross-linked duplex (0.6 nmol). Digestions were carried out at 37 °C for 50 min. Collected fractions were analyzed by MALDI-TOF MS.

It was further confirmed that in all cases, cross-linking with **2** preferably occurs to the opposing base leaving the neighboring bases in the complementary strand mainly untouched.[54]

As for cross-link reactions through building block **3**, Figure 10 shows analysis data for the representative example of duplex **D3b**. Incorporation of the cyclic furan-containing building block **3** apparently causes less severe duplex distortion as indicated by the complete absence of the tailed compounds (cfr Figure 9), indicating a smoother recognition and degradation of the duplex. Moreover EXO III can approach the modified residue more closely as indicated by the fragment represented in Figure 10b. The additional isolation of the fragment shown in Figure 10c further shows that the nu-

  

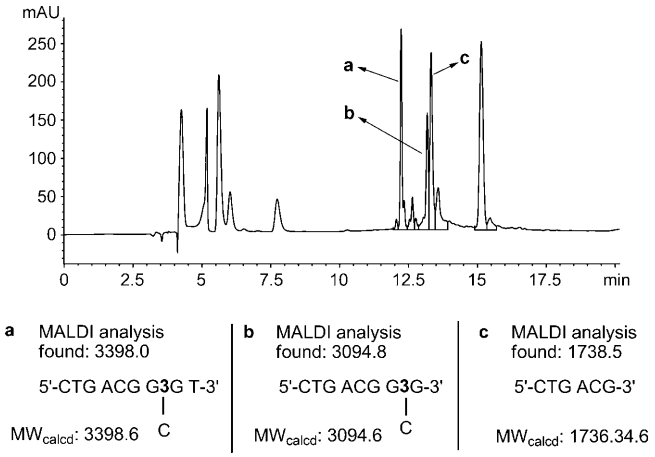


Figure 10. Reverse-phase HPLC chromatogram after EXO III digestion of duplex **D3b** d(CTGACGG**3**GTGC:GACTGCCCCACG). Enzymatic degradation was performed using 200 units of EXOIII for purified cross-linked duplex (0.6 nmol). Digestions were carried out at 37 °C for 50 min. Collected fractions were analyzed by MALDI-TOF MS.

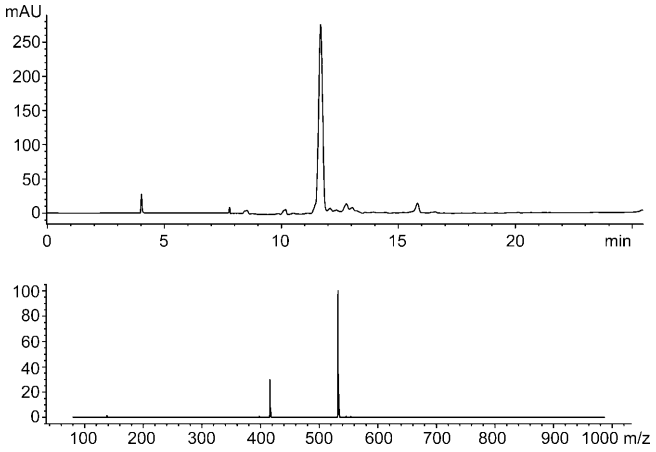


Figure 11. Reverse-phase HPLC (top) and ESI-MS (bottom) data of purified dinucleoside **13**.

clease can degrade even beyond the modified residue. As such, comparison of digestion fragments between **D2** and **D3** duplexes can be interpreted in terms of a better recognition of duplexes containing cyclic building block **3** by the natural enzyme.

**Detailed structural characterization of the cross-linked species**: Although the described experiments yield information about the exact location of the cross-link and the selectivity of the specific furan-modified building block involved, no direct structural information as to the exact chemical structure of the cross-linked species can be deducted. Similar to our previous studies,[12] a solution experiment on the nucleoside level was carried out involving NBS oxidation of protected furan analogue **5** in the presence of deoxycytidine.

The obtained crude dinucleoside was purified by flash chromatography and the resulting compound was analyzed by reverse-phase HPLC/MS and NMR spectroscopy (see Supporting Information for experimental procedures and NMR data). Isolation of the product resulted in clean reverse-phase HPLC and MS spectra (Figure 11). The signal at *m*/*z* 532 corresponds to the protonated $[M+H]^+$ cross-linked product **13** and *m*/*z* 416 corresponds to a compound in which the glycosidic bond has been cleaved and in which only the cytosine base is attached to the oxidized cross-link residue.

The obtained $^1$H NMR spectrum, indicating the presence of a mixture of stereoisomers, was compared with literature data[55] for the earlier characterized natural adduct of *cis*-butenedial and dC. The proposed pathway for cross-link formation thus is again suggested to involve the initial attack of the exocyclic amine on the aldehyde of the generated enal functionality, followed by a rearrangement leading to Michael addition on the remainder of the oxidized furan moiety (Scheme 5). As such the isolated adduct proves to be structurally similar to the dC adduct of the formal C4′-oxidized abasic site β-elimination product isolated by Ravanat, Cadet, and co-workers.[56]

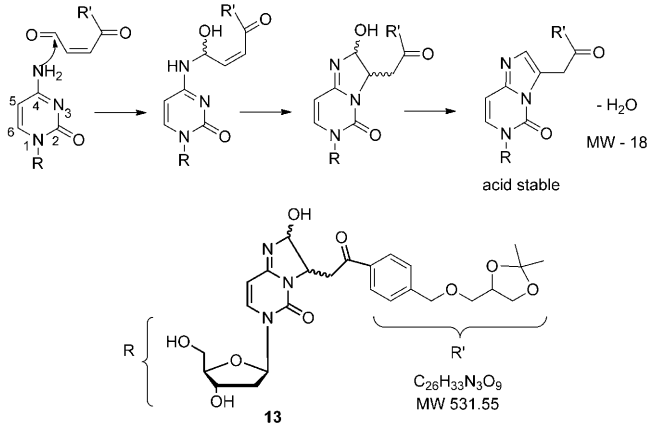


Scheme 5. Structural characterization of the cross-linked species through generation of a cross-linked dinucleoside.

## Conclusion

The exact nature of the furan-containing building block used in the current furan-oxidation cross-linking method has a considerable influence on the yield and chemoselectivity of the cross-link formation through the generated enal functionality. A delicate interplay between electronic and steric factors can be observed. Although the enlargement of the aromatic system within the phenyl–furan building blocks has a beneficial influence on duplex stability, the altered electronic nature of the furan moiety promotes a bromination side reaction that negatively influences the yield. For a more in depth comprehension of the experimental results theoretical calculations were carried out. As the duplex structure is important in the study of ICL repair studies, the presented molecular modeling studies shed light on the structural con-

  

sequences of introducing cyclic or acyclic building blocks. Rather than duplex stability, the precise orientation of the modified building block seems to play an important role in achieving selective cross-linking to one specific complementary base, as the observed localization of the furan moiety coincides well with the observed cross-link selectivity. Furthermore, calculations have illustrated the role of the phenyl moiety in the bromination side reaction. The structural exploration conducted to date, with a gradually increasing building block complexity, allows us to define some of the parameters important for achieving acceptable yields and cross-link selectivity.

In terms of a homogeneous diagnosis of a cytosine-related one-point variation within DNA, the observed C selectivity represents a remarkable advantage of cross-linking by cyclic furan derivative **3**. Whereas all previous furan-decorated moieties in general form covalent bonds with A or C complements, cyclic derivative **3** exhibits a rather pronounced selectivity for cross-linking to one specific complementary base. The method described herein constitutes one of the few methodologies for site specific ICL formation in the major groove. Furthermore, as indicated by enzymatic digestion studies, cross-linking through **3** results in a less distorted duplex, which possibly is an important factor for recognition of cross-linked model duplexes by natural enzymes.

It can be concluded from the current work that restricted mobility, though causing duplex destabilization, can have a beneficial influence on the selectivity of the cross-link reaction. Although the phenyl–furan moiety utilized here does give rise to an undesired side reaction, a clear stabilizing influence on the duplex can be noted when comparing to the acyclic furan-based system **1**. Duplexes incorporating either the building block **2** or **3** have been shown to be more stable, in the range 5–15 °C, than the ones incorporating the acyclic furan-containing counterpart.

In conclusion, the cyclic phenyl–furan-containing building block shows a somewhat lower but still very appreciable isolated yield of cross-linked duplex; however, its selectivity towards cross-linking with C is considerably higher than in the previous series. Given the modular nature of our building block synthesis and the commercial availability of various furan derivatives, the current study demonstrates that the furan-oxidation cross-link strategy allows fine-tuning of selectivity by the precise choice and conformational behavior of the modified furan-containing moiety.

## Experimental Section

**Materials and methods for chemical synthesis**: All solvents and chemical reagents were purchased from Sigma–Aldrich. $^{1}$H NMR and $^{13}$C NMR spectra were recorded on a Bruker Avance 300 or a Bruker DRX 500 spectrometer operating at room temperature. Chemical shifts are reported in parts per million ($\delta$) relative to the residual solvent peak. Multiplicities are reported as singlet (s), doublet (d), doublet of doublets (dd), triplet (t) or multiplet (m). Purities of small compounds were checked by reverse-phase HPLC-MS or by reverse-phase HPLC. Reverse-phase HPLC-MS: Agilent-1100 series LC/MS system equipped with a Phenomenex Luna C18 column (250×4.6 mm, 5 μ at 35 °C). The used solvent system was 5 mM $NH_4OAC$ in water (A) and MeCN (B). The used gradient went from 0 to 100 % B in 15 min. Reverse-phase HPLC: Agilent 1100 system equipped with a Phenomenex Luna C18 column (250× 4.6 mm, 5 μ, at 50 °C) with 0.1 M TEAA (containing 8 % MeOH) and MeOH as mobile phase (linear gradient: 0–30 % MeOH in 15 min, 30–100 % MeOH in 3 min).

**Synthesis of nucleoside building blocks**

(*S*)-1-[Bis(4-methoxyphenyl)phenylmethoxy]-3-(4-furan-2-ylbenzyloxy)-propan-2-ol (6): See Supporting Information for detailed procedures, analysis data, and NMR spectra:

**Diisopropylphosphoramidous acid 2-[bis(4-methoxyphenyl)methoxy]-1-(4-furan-2-ylbenzyloxymethyl)ethyl ester 2-cyanoethyl ester (7)**: Compound **6** (100 mg, 0.18 mmol) was dissolved in fresh distilled $CH_2Cl_2$ (6 mL) under argon atmosphere. *N*,*N*-Diisopropylammoniumtetrazolide (46 mg, 0.27 mmol, 1.5 equiv) was added and the resulting mixture was stirred at room temperature. 2-Cyanoethyltetraisopropylphosphoramidite (60 mg, 0.2 mmol, 1.1 equiv) was added, while cooling on an ice-bath and the reaction mixture was allowed to stir overnight at room temperature. When no further conversion occurred, the reaction mixture was quenched with MeOH (4 mL). The solvent was partially evaporated and water was added. The product was extracted with $CH_2Cl_2$, dried on anhydrous $Na_2SO_4$, and the solvent was removed under reduced pressure. The residue was purified using Merck silica gel (2:8 EtOAc/petroleum ether with 1 % $Et_3N$) to yield **7** (106 mg, 79 %) ($R_f$ = 0.32 (2:7 EtOAc/petroleum ether)). This product was used in the oligonucleotide synthesis. IR (KBr-film): $\tilde{\nu}$ = 2928, 1608, 1508, 1302, 1176, 829 cm$^{-1}$; UV: $\lambda_{max}$ = 285 nm ($H_2O$/ACN); LRMS (ESI-MS): *m*/*z* calcd for $C_{44}H_{51}N_2O_7P$: 750.3, found: 773.7 $[M+Na]^+$; $^{31}$P NMR (121 MHz, $CDCl_3$): $\delta$ = 149.44, 149.62 ppm.

**2-[Bis-(4-methoxyphenyl)phenylmethoxymethyl]-5-(4-furan-2-ylphenyl)-tetrahydrofuran-3-ol (11):** See Supporting Information for detailed procedures, analysis data and NMR spectra.

**Diisopropylphosphoramidous acid 2-[bis-(4-methoxyphenyl)phenylmethoxymethyl]-5-(4-furan-2-ylphenyl)tetrahydrofuran-3-yl ester 2-cyanoethyl ester (12)**: Nucleoside 11 (90 mg, 0.16 mmol) was dissolved in dry $CH_2Cl_2$ (3 mL) and *N*,-diisopropylethylamine (0.25 mL) was added. ($i$Pr$_2$N)(NCCH$_2$CH$_2$O)PCl (95 mg, 0.4 mmol, 2.5 equiv) was added in one portion and the resulting mixture was stirred at room temperature. After 2 h the reaction was quenched by addition of MeOH (2 mL), stirred for another 15 min, followed by addition of saturated $NaHCO_3$ solution (3 mL). This mixture was extracted three times with $CH_2Cl_2$. The organic layer was dried over $Na_2SO_4$ and evaporated under reduced pressure. The reaction mixture was purified by column chromatography with 4:1 isooctane:EtOAc (1 % TEA). The product was collected as a yellow oil (70 mg, 0.091 mmol, 59 %). $R_f$ = 0.30 (7:2 petroleum ether/EtOAc). $^{31}$P NMR (121 MHz, $CDCl_3$): $\delta$ = 147.98, 148.16 ppm.

**Materials and methods for oligonucleotides**: Reagents for DNA synthesis were obtained from Glen Research. All reverse-phase HPLC experiments with oligonucleotides were recorded on an Agilent 1100 system equipped with a Phenomenex Clarity column (250×4.6 mm, 5 μ) at 50 °C with 0.1 M TEAA (with 5 % MeCN) and MeCN as mobile phase (linear gradient: 0–30 % MeCN in 15 min). When stated the same conditions were used with a Jupiter 300 Å column (250×4.6 mm, 5 μm). The chromatograms were analyzed at 260 nm. Enzymatic digestion reaction mixtures were analyzed on a Phenomenex Luna C18 column (250×4.6 mm, 5 μ) using the same method. HPLC-purified samples were subjected to MALDI-TOF analysis. MALDI-TOF spectra were recorded in positive mode on an Applied Biosystems voyager DE-STR biospectrometry workstation. The matrix was a mixture of 0.7 M 3-hydroxypicolinic acid and 0.07 M ammoniumcitrate for adduct suppression. The samples were desalted by addition of small amounts DOWEX beads which were thoroughly rinsed with water before use. This was done in the sample tube and not on the sample plate as in certain cases (if $NaCNBH_3$ was present) the sample plate corroded and presence of DOWEX beads resulted in amorphous drying instead of crystallization.

**Synthesis of modified DNA**: All oligonucleotides were synthesized DMT-on using an ABI 394 DNA-synthesizer at 1 μmol scales. A standard synthesis protocol was used except for coupling of the modified residues.

  

The synthesis column was removed from the DNA-synthesizer for the introduction of the modified residues. For these manual couplings, a 0.06 M solution of the phosphoramidite in acetonitrile and a 0.1 M solution of dicyanoimidazole (DCI) in acetonitrile were dried on molecular sieves for about 20 min. Then small portions of the phosphoramidite solution (0.4 mL) and the DCI solution (0.5 mL) were alternately pushed through the reaction column. The column was flushed with acetonitrile (1 mL) and a mixture of Cap A (0.5 mL) and Cap B (0.5 mL) was pushed through the column, after which it was again flushed with acetonitrile (1 mL). The column was reinstalled on the DNA-synthesizer and automated synthesis was resumed.

Oligonucleotides were cleaved from solid support and deprotected by incubation at 55 °C overnight in concentrated aqueous ammonia. The synthesized DMTr-ON oligonucleotides were deprotected and purified on Sep-pak C18 cartridges (obtained from Waters).

**Thermal denaturation experiments**: All UV experiments were recorded on a Varian Cary 300 Bio equipped with a six-cell thermostatted cell holder. Concentrations were measured at 260 nm for all oligonucleotides at room temperature. Extinction coefficients ($\varepsilon$) were calculated according to the nearest neighbour method. Melting curves were monitored at 260 nm with a heating rate of 0.3 °C $min^{-1}$. The buffer contained 100 mM NaCl and 10 mM phosphate buffer (pH 7). Oligonucleotide concentration was 2 μM for each strand. Melting temperatures were calculated from the first derivative of the heating curves using the Cary 300 Bio software.

**Cross-linking reactions**: The modified strands were mixed with their complements in equimolar amounts at 0.02 mM concentration in 10 mM phosphate buffer (pH 7) and 100 mM NaCl before annealing from 95 °C to room temperature. The final concentration of oligonucleotide duplex was 20 μM. Temperatures during the whole reaction were kept constant in an Eppendorf thermomixer comfort at 20 °C. A stock solution of NBS in $H_2O$ (1 equiv/2 μL) was freshly prepared and to start the reaction, one equivalent NBS was added. This was repeated every 15 min until complete disappearance of the modified oligonucleotide. The reactions were monitored by RP-HPLC.

**Gel-electrophoresis experiments**: A 20% polyacrylamide (acrylamide: bisacrylamide 19:1) with 1X TBE buffer and 7 M urea was used for all analyses. The temperature of the gel was stabilized with a Julabo F12 at 25 °C. The power supply used for gel-electrophoresis was a consort EV202. Gels were stained with GelRed (VWR) and pictures were taken with an Autochemi imaging system (UVP).

**Enzymatic digestion**: Exonuclease III was purchased from GE healthcare or Sigma. For the enzymatic degradations the cross-linked duplex (0.6 nmol) was dissolved in 1X reaction buffer (66 or 88 μL) supplied with the enzyme. Then, 200 units of the enzyme were added and the mixture was shaken at 37 °C for 55 min. The reaction mixture was injected immediately onto reverse-phase HPLC for purification and the peaks eluting after 7 min were collected. Those eluting faster correspond to mononucleotides from the digestion.

## Acknowledgements

K.S. is indebted to the Special Research Fund of Ghent University (BOF-GOA2007, BOF-BAS 01B04405). This research project has further been supported by a Marie Curie Early Stage Research Training Fellowship of the European Community's Sixth Framework Programme under contract number MEST-CT-2005-020643. M.H. is indebted to the Academy of Sciences of the Czech Republic (Z4 055 905), to the Ministry of Education of the Czech Republic (LC 512), and to the Grant Agency of the ASCR (IAA400550902). A.M. further thanks the FWO Vlaanderen for financial support (FWO-KAN 1.5.137.09N, FWO-KAN 1.5.186-03). Computational resources and services used in this work were provided by Ghent University.

[1] G. J. Moser, J. Foley, M. Burnett, T. L. Goldsworthy, R. Maronpot, *Exp. Toxicol. Pathol.* **2009**, *61*, 101–111.
[2] A. E. Sirica, *Toxicol. Pathol.* **1996**, *24*, 90–99.
[3] R. Fransson-steen, T. L. Goldsworthy, G. L. Kedderis, R. Maronpot, *Toxicology* **1997**, *118*, 195–204.
[4] D. Lu, L. A. Peterson, *Chem. Res. Toxicol.* **2010**, *23*, 142–151.
[5] D. Lu, M. M. Sullivan, M. B. Phillips, L. A. Peterson, *Chem. Res. Toxicol.* **2009**, *22*, 997–1007.
[6] L. A. Peterson, M. E. Cummings, J. Y. Chan, C. C. Vu, B. A. Matter, *Chem. Res. Toxicol.* **2006**, *19*, 1138–1141.
[7] K. C. Hickling, J. M. Hitchcock, V. Oreffo, A. Mally, T. G. Hammond, J. G. Evans, J. K. Chipman, *Toxicol. Pathol.* **2010**, *38*, 230–243.
[8] Y. Kobayashi, G. B. Kumar, T. Kurachi, H. P. Acharya, T. Yamazaki, T. Kitazume, *J. Org. Chem.* **2001**, *66*, 2011–2018.
[9] Y. Kobayashi, M. Nakano, H. Okui, *Tetrahedron Lett.* **1997**, *38*, 8883–8886.
[10] M. D. Burke, E. M. Berger, S. L. Schreiber, *Science* **2003**, *302*, 613–618.
[11] a) S. Halila, T. Velasco, P. De Clercq, A. Madder, *Chem. Commun.* **2005**, 936–938; b) M. Op de Beeck, A. Madder, *J. Am. Chem. Soc.* **2011**, *133*, 796–807.
[12] K. Stevens, A. Madder, *Nucleic Acids Res.* **2009**, *37*, 1555–1565.
[13] S. S. Lange, M. C. Reddy, K. M. Vasquez, *DNA Repair* **2009**, *8*, 865–872.
[14] K. M. Mccabe, S. B. Olson, R. E. Moses, *J. Cell. Physiol.* **2009**, *220*, 569–573.
[15] K. Tsuchida, K. Komatsu, *Cancer Sci.* **2008**, *99*, 2238–2243.
[16] O. D. Schärer, *ChemBioChem* **2005**, *6*, 27–32.
[17] J. T. Millard, S. Raucher, P. B. Hopkins, *J. Am. Chem. Soc.* **1990**, *112*, 2459–2460.
[18] P. L. Fischhaber, A. S. Gall, J. A. Duncan, P. B. Hopkins, *Cancer Res.* **1999**, *59*, 4363–4368.
[19] A. J. Warren, J. W. Hamilton, *Chem. Res. Toxicol.* **1996**, *9*, 1063–1071.
[20] D. M. Noll, A. M. Noronha, P. S. Miller, *J. Am. Chem. Soc.* **2001**, *123*, 3405–3411.
[21] C. J. Wilds, A. M. Noronha, S. Robidoux, P. S. Miller, *J. Am. Chem. Soc.* **2004**, *126*, 9257–9265.
[22] C. J. Wilds, F. Xu, A. M. Noronha, *Chem. Res. Toxicol.* **2008**, *21*, 686–695.
[23] T. Angelov, A. Guainazzi, O. D. Scharer, *Org. Lett.* **2009**, *11*, 661–664.
[24] Y. Taniguchi, Y. Kurose, T. Nishioka, F. Nagatsugi, S. Sasaki, *Bioorg. Med. Chem.* **2010**, *18*, 2894–2901.
[25] A. Murakami, Y. Yamamoto, M. Namba, R. Iwase, T. Yamaoka, *Bioorg. Chem.* **2001**, *29*, 223–233.
[26] M. Nakane, S. Ichikawa, A. Matsuda, *J. Org. Chem.* **2008**, *73*, 1842–1851.
[27] M. Comb, N. Mermod, S. E. Hyman, J. Pearlberg, M. E. Ross, H. M. Goodman, *EMBO J.* **1988**, *7*, 3793–3805.
[28] S. Murata, Y. Mizumura, K. Hino, Y. S. Ichikawa, A. Matsuda, *J. Am. Chem. Soc.* **2007**, *129*, 10300–10301.
[29] M. Endo, T. Majima, *Org. Biomol. Chem.* **2005**, *3*, 3476–3478.
[30] M. Ogino, K. Fujimoto, *Angew. Chem.* **2006**, *118*, 7381–7384; *Angew. Chem. Int. Ed.* **2006**, *45*, 7223–7226.
[31] H. Y. Li, Y. L. Qiu, E. Moyroud, Y. Kishi, *Angew. Chem.* **2001**, *113*, 1519–1523; *Angew. Chem. Int. Ed.* **2001**, *40*, 1471–1475.
[32] a) Q. B. Zhou, S. E. Rokita, *Proc. Natl. Acad. Sci. USA* **2003**, *100*, 15452–15457; b) J. T. Sczepanski, A. C. Jacobs, M. M. Greenberg, *J. Am. Chem. Soc.* **2008**, *130*, 9646–9647; c) X. Peng, I. S. Hong, H. Li, M. M. Seidman, M. M. Greenberg, *J. Am. Chem. Soc.* **2008**, *130*, 10299–10306; d) T. Kawasaki, F. Nagatsugi, A. Monsur, M. Maeda, K. Sugiyama, K. Hori, S. Sasaki, *J. Org. Chem.* **2005**, *70*, 14–23.
[33] A. Kobori, J. Morita, M. Ikeda, A. Yamayoshi, A. Murakami, *Bioorg. Med. Chem. Lett.* **2009**, *19*, 3657–3660.
[34] M. B. Smeaton, E. M. Hlavin, A. M. Noronha, S. P. Murphy, C. J. Wilds, P. S. Miller, *Chem. Res. Toxicol.* **2009**, *22*, 1285–1297.

  

[35] M. Štefko, R. Pohl, B. Klepetářová, M. Hocek, *Eur. J. Org. Chem.* **2008**, *73*, 1689–1704.
[36] M. Urban, R. Pohl, B. Klepetářová, M. Hocek, *J. Org. Chem.* **2006**, *71*, 7322–7328.
[37] N. Joubert, R. Pohl, B. Klepetářová, M. Hocek, *J. Org. Chem.* **2007**, *72*, 6797–6805.
[38] J. Bárta, R. Pohl, B. Klepetářová, N. P. Ernsting, M. Hocek, *J. Org. Chem.* **2008**, *73*, 3798–3806.
[39] M. Štefko, R. Pohl, M. Hocek, *Tetrahedron* **2009**, *65*, 4471–4483.
[40] M. Štefko, L. Slavětínská, B. Klepetářová, M. Hocek, *J. Org. Chem.* **2010**, *75*, 442–449.
[41] M. Hocek, R. Pohl, B. Klepetářová, *Eur. J. Org. Chem.* **2005**, 4525–4528.
[42] N. Joubert, M. Urban, R. Pohl, M. Hocek, *Synthesis* **2008**, 1918–1932.
[43] C. Vargeese, J. Carter, J. Yegge, S. Krivjanski, A. Settle, E. Kropp, K. Peterson, W. Pieken, *Nucleic Acids Res.* **1998**, *26*, 1046–1050.
[44] Figure 1 graphically summarizes $T_m$ results for duplexes incorporating two A residues neighboring the modified residue. Similar results and conclusions apply for duplexes incorporating any of the other three residues at the neighboring positions (see data in Table 1).
[45] D. A. Case, T. A. Darden, T. E. Cheatham, III, C. L. Simmerling, J. Wang, R. E. Duke, R. Luo, K. M. Merz, D. A. Pearlman, M. Crowley, R. C. Walker, W. Zhang, B. Wang, S. Hayik, A. Roitberg, G. Seabra, K. F. Wong, F. Paesani, X. Wu, S. Brozell, V. Tsui, H. Gohlke, L. Yang, C. Tan, J. Mongan, V. Hornak, G. Cui, P. Beroza, D. H. Mathews, C. Schafmeister, W. S. Ross, P. A. Kollman, AMBER 9, University of California, San Francisco, **2006**.
[46] D. A. Case, T. Cheatham, T. Darden, H. Gohlke, R. Luo, K. M. Merz, Jr., A. Onufriev, C. Simmerling, B. Wang, R. Woods, *J. Comput. Chem.* **2005**, *26*, 1668–1688.
[47] L. Zendlová, D. řeha, M. Hocek, P. Hobza, *Chem. Eur. J.* **2009**, *15*, 7601–7610.
[48] I. Singh, W. Hecker, A. K. Prasad, V. S. Parmar, O. Seitz, *Chem. Commun.* **2002**, 500–501.
[49] J. T. Sczepanski, A. C. Jacobs, A. Majumdar, M. M. Greenberg, *J. Am. Chem. Soc.* **2009**, *131*, 11132–11139.
[50] Z. Wang, K. X. Wan, R. Ramanathan, J. S. Taylor, M. L. Gross, *J. Am. Soc. Mass Spectrom.* **1998**, *9*, 683–691.
[51] Mechanistic details of furan oxidation with NBS in water.

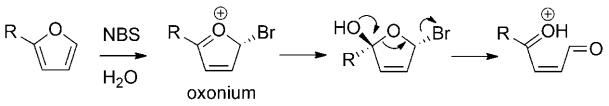


[52] Y. Kobayashi, M. Nakano, G. B. Kumar, K. Kishihara, *J. Org. Chem.* **1998**, *63*, 7505–7515.
[53] A. Machwe, R. Ganunis, V. A. Bohr, D. K. Orren, *Nucleic Acids Res.* **2000**, *28*, 2762–2770.
[54] Only in case of duplex **D2b** ($G_7$**2**$G_9$:$C_{18}C_{17}C_{16}$ sequence context), MALDI-TOF analysis revealed the presence of a minor amount of cross-linked product containing a covalent bond to the neighboring $C_{16}$ through the isolation of the corresponding tailed compound.
[55] L. Gingipalli, P. C. Dedon, *J. Am. Chem. Soc.* **2001**, *123*, 2664–2665.
[56] P. Regulus, B. Duroux, P. A. Baylet, A. Favier, J. Cadet, J. L. Ravanat, *Proc. Natl. Acad. Sci. USA* **2007**, *104*, 14032–14037.

Received: January 7, 2011
Published online: May 20, 2011

  